Supplementary Information for

Specific contribution of Reelin expressed by Cajal-Retzius cells or GABAergic interneurons to cortical lamination

Alba Vílchez-Acosta, Yasmina Manso, Adrián Cárdenas, Alba Elias-Tersa, Magdalena Martínez-Losa, Marta Pascual, Manuel Álvarez-Dolado, Angus C. Nairn, Víctor Borrell and Eduardo Soriano

Email: esoriano@ub.edu

This PDF file includes:

Extended Methods

Figures S1 to S11

Extended Methods

Animals

To generate the Floxed Reelin (*Reelin*$^{F/F}$) line, the MluI-Eco47III cloning vector (13914 bp) was used to create a targeting vector that contained the exon 1 of the Reelin sequence flanked by LoxP sites and downstream and upstream genomic sequences for homologous recombination **(SI Appendix Fig. S1*A*)**. The definitive construct was linearized and electroporated into embryonic stem (ES) cells and gene-targeting was verified by Southern blot and PCR. Chimeric founder mice were obtained by injection of ES cells harboring the floxed Reelin allele into C57Bl/6J blastocysts. Chimeras were crossed with C57Bl/6J mice and the resulting offspring (heterozygous floxed Reelin mice, *Reelin*$^{F/WT}$) were backcrossed to obtain homozygous floxed Reelin mice (*Reelin*$^{F/F}$) in a C57/Bl6 background.

Floxed Reelin (*Reelin*$^{F/F}$) mice, in which exon 1 of the Reelin gene is flanked by loxP sequences, were crossed with cell-specific constitutive Cre recombinase mice to obtain double transgenic mice with specific deletion of the Reelin gene either in Cajal-Retzius cells or GABAergic interneurons (1). In the first case, Cre recombinase expression was under the control of the Calretinin promoter (*Calb2*$^{tm1(cre)Zjh}$/J, stock #010774, The Jackson Laboratory) and the resulting offspring were homozygous for floxed Reelin (*Reelin*$^{F/F}$) and either had 2 copies of Cre (*CR-Reelin*$^{F/F}$), 1 copy (heterozygous) or none (*Reelin*$^{F/F}$). In the second case, Cre recombinase was under the control of the Gad2 promoter (*Gad2*$^{tm2(cre)Zjh}$/J, stock #010802, The Jackson Laboratory) and the resulting offspring were homozygous for floxed Reelin and either had 2 copies of Cre (*GAD-Reelin*$^{F/F}$), 1 copy (heterozygous) or none (*Reelin*$^{F/F}$). In both lines, only Cre homozygous (*CR-Reelin*$^{F/F}$ and *GAD-Reelin*$^{F/F}$) mice and those without Cre (*Reelin*$^{F/F}$) were used for experimental purposes, while the heterozygous animals were used for breeding purposes. All mice were kept in a C57BL/6J background and housed in groups in a 12 h light/dark cycle with free access to water and food. All procedures were performed with mice of both genders, following the guidelines of the European Community Directive 2010/63/EU, and were approved by the Ethics Committee for Animal Experimentation of the University of Barcelona (CEEA, Barcelona, Spain).

PCR

Genomic DNA was extracted from mouse tail tips and standard PCR amplification was performed. To determine the number of floxed Reelin alleles, the following primers were used: A 5’ CGA GGT GCT CAT TTC CCT GCA CAT TGC 3’ and B 5’ CAC CGA CCA AAG TGC TCC AAT CTG TCG 3’. In mice homozygous for floxed Reelin (*Reelin*$^{F/F}$), a single band at 613 bp was amplified.

Mice heterozygous for floxed Reelin (*Reelin*$^{F/WT}$) had an additional band at 496 bp. To determine the number of Cre copies, a standard PCR amplification following The Jackson Laboratory's guidelines was performed. For the CR line, the following primers were used: Common 5' AGG TCT GGG AAG GAG TGT CA 3'; Mutant Forward 5' CCA CTA GAT CGA ATT CCG AAG 5' and Wild-Type Forward 3' ACC TGG AGA TTG TGC TCT GC 3'. In the *CR-Reelin*$^{F/F}$ mice, a single 175-bp band was amplified while a 125-bp band was amplified in the Reelin$^{F/F}$ mice. Both bands were amplified in the heterozygous mice. For the Gad line, the following primers were used: Common 5' CAC CCC ACT GGT TTT GAT TT 3'; Mutant Forward 5' AAA GCA ATA GCA TCA CAA ATT TCA 3' and Wild-Type Forward 5' CTT CTT CCG CAT GGT CAT CT 3'. A 352-bp band and 250-bp band was amplified in the *GAD-Reelin*$^{F/F}$ and *Reelin*$^{F/F}$ mice, respectively. Both bands were amplified in the heterozygous animals.

Antibodies and Reagents

The following commercial primary antibodies were used for immunohistochemistry: Anti-Reelin (clone G10, MAB5364, Millipore, 1:500); Anti-Cux1 (SC-13024, Santa Cruz Biotechnology, 1:250); Anti-CTIP2 (ab18465, Abcam, 1:500); Anti-BrdU (OBT0030, Axyll, 1:250 and Clone BU1/75 ab6326, Abcam, 1:250); Anti-Calretinin (7699/3H, Swant Antibodies, 1:1000); Anti-NeuN (MAB377B, Millipore, 1:500); Anti-GAD65/67 (AB1511, Chemicon International, 1:1000); Anti-GFP (GFP 1020, Aves Lab, 1:500); and Anti-Prox1 (1:10.000, kind gift from Dr. S. Pleasure, University of California, San Francisco). For western blot, Anti-β-III-Tubulin (MMS-435P, Covance) was used.

Alexa Fluor Fluorescent secondary antibodies were from Invitrogen. Biotinylated-secondary antibodies were from Vector Labs. The streptavidin-biotinylated/HRP complex and ECL were supplied by GE Healthcare. The F(ab')$_2$ fragment anti-mouse IgG (1:300) was from Jackson ImmunoResearch. The HRP-labeled secondary antibodies used for western blot were provided by DAKO. BrdU, Hoechst 33342, diaminobenzidine reagent (DAB) and Eukitt mounting media were from Sigma-Aldrich. Mowiol was from Calbiochem. The BCA Protein Assay was from Thermo Fisher.

Tissue Processing and Immunohistochemistry

Embryonic tissue (E12, E16) was fixed by immersion in 4% Paraformaldehyde (PFA) in 0.1 M phosphate buffer (PB) for 24 h at 4°C, cryoprotected with PBS-30% sucrose, frozen in 2-methyl butane at ~-42°C, coronally sectioned on a cryostat (Leica CM1900) at 15 microns and collected on Superfrost Plus slides (Thermo Scientific). Tissue slides were kept at -20°C until use. Late embryos (E18-19) and postnatal mice (P1, P15, and P30) were deeply anaesthetized and

transcardially perfused with 4% PFA in 0.1 M PBS. After perfusion, the brain was quickly removed from the skull and post-fixed for 24 h at 4°C. Brains were then cryoprotected with PBS-30% sucrose, frozen, coronally sliced on a freezing microtome (Leica SM2010R) at 30 (P15 and P30) or 50 µm (P1, E18, E19), and distributed in either 10 or 6 series, respectively. Tissue was kept in cryoprotective medium at -20°C until use.

For immunodetection, brain sections were blocked for 2 h at Room Temperature (RT) with 10% Normal Goat/Horse Serum (NGS or NHS), 0.2% gelatin and $F(ab')_2$ fragment anti-mouse unconjugated IgG (1:300) when necessary. For BrdU and CTIP2 detection, heat-mediated antigen retrieval was performed before the blocking. Primary antibodies were incubated overnight at 4°C. For immunofluorescence, sections were incubated for 2 h at RT with Alexa Fluor secondary antibodies (1:500) in PBS–5% NGS or NHS and then counterstained with Hoechst for nucleus detection. Sections were then mounted in Mowiol and stored at −20°C. For immunohistochemistry, sequential incubation with biotinylated secondary antibodies (1:200; 2 h at RT) and streptavidin-HRP (1:400; 2 h at RT) was performed in PBS–5% NGS/NHS. The staining was developed using DAB and H_2O_2. Finally, sections were dehydrated and mounted with Eukitt.

Western Blot

Mice were killed by decapitation and the brain was quickly removed from the skull. The brain was split into hemispheres and the cortex and hippocampus of each hemisphere were quickly dissected, frozen in liquid nitrogen and stored at -80°C until use. Brain tissue was processed as previously described (2). Briefly, brains were homogenized in lysis buffer using a Polytron and then sonicated and centrifuged to remove insoluble debris. The supernatant was collected and stored at -20°C until use. A small fraction of the supernatant was used to determine protein concentration using the BCA protein assay. Samples were resolved by SDS-polyacrylamide gels and transferred onto nitrocellulose membranes. Membranes were then blocked for 2 h at RT in TBST containing 5% non-fat milk. Reelin primary antibody was incubated overnight at 4°C (1:4000) whilst Tubulin antibody (1:100.000) was incubated for 30 min RT. After incubation with secondary HRP-labeled antibodies for 1 h at RT (1:2000), membranes were developed with the ECL system.

BrdU Administration

Pregnant females from timed mating crossings were given two pulses of BrdU (50 mg/Kg; 2-h interval between injections) at Embryonic day (E) 12 and 15 to label the lower and upper cortical layer cells, respectively. The day the vaginal plug was detected was considered as E0. The resulting offspring were sacrificed at P30 and tissue was collected for

immunohistochemistry, as previously described in the methods section. For postnatal administration, pups were injected with BrdU (50 mg/Kg) at P10 and P11 and were later killed at P30. Tissue was collected for immunohistochemistry as previously described.

Electroporation

Mouse embryos were electroporated in utero at E14.5 as previously described (3). Briefly, pregnant females were deeply anesthetized with isoflurane. The uterine horns were exposed and GFP (plasmid) under the control of CAG promoter was injected into the ventricular zone of the embryos using pulled glass micropipettes. Square electric pulses (28-35V, 50 ms on – 950 ms off, 5 pulses) were applied with an electric stimulator (Cuy21EDIT Bex C., LTD) using round electrodes (CUY650P5, Nepa Gene). At P1, pups were perfused with 4% PFA and the brain was quickly removed and post-fixed for 24 h at 4°C. E18-E19 embryos were processed as above. The tissue was then cryoprotected with PBS-30% sucrose, frozen, and sliced at 50 microns in a Leica cryostat. Slides were kept at -20°C until use.

Transplantation experiments

MGE transplantations were done as described (4). E13.5 C57Bl/6J /GFP+ (5) embryos were placed in DMEM/F12 medium, GIBCO™, and the ventricular and subventricular zones of the anterior part of the MGE were dissected as described (6, 7). At E13.5, the density of MGE embryonic interneuron progenitors is at its peak, and the MGE is clearly delineated by a sulcus from the lateral ganglionic eminence (LGE). Tissue explants were collected in DMEM/F12 medium and dissociated containing DNase I (10–100 mg/ml) and mechanically dissociated by repeated pipetting through a 200 mL plastic tip. MGE cell number and viability (80%) were determined by trypan blue exclusion. The cells were pelleted by centrifugation (5 min, 300x g) and resuspended in DMEM/F12 medium. MGE cell suspensions were front loaded into beveled glass micropipettes. For stereotaxic injections, P3 mice were anesthetized by hypothermia induced by placement on ice until the pedal reflex was abolished. A microinjector and stereotaxic frame were used to deliver a total of $2x10^5$ MGE cells per mouse distributed unilaterally (right hemisphere) across 4 cortical points (50–100 nL per site) through 2 injection sites. Stereotaxic coordinates were the following: for anterior injection sites, -3 from the naison at a 30º angle; L +3.0 ; D -0.70 and -0.20 (from the skull surface); for posterior injection sites, A -4 from the naison at a 30º angle; L +3.0; D -0.70 and -0,20 (from the skull surface). P18 mice were perfused and processed for immunohistochemistry as above.

Image Acquisition and Data Analysis

Bright-field images were acquired with an Olympus D72 camera attached to a Nikon Eclipse E600 microscope and with a NanoZoomer 2.0-HT (Hamamatsu Photonics). Fluorescent images were taken using a Leica TCS SP5 confocal microscope, a Nikon Eclipse E600 microscope, a NanoZoomer 2.0-HT and a Leica thunder DMi8 microscope attached to a Leica K5, SCMOS camera. Image processing was done with FIJI (Image J). To determine the layer distribution of cells in the cortex (Cux1 for upper layers, CTIP2 for lower layers, BrdU and GFP), images from the Primary Somatosensory Barrel Field (SBF1) were taken using 10x, 20x and 40x oil-immersion objectives on a Leica TCS SP5 confocal microscope (Cux1 and CTIP2), a Nikon Eclipse E600 microscope (BrdU) and a NanoZoomer 2.0-HT (GFP). For each mouse, 9 Regions of Interest (ROIs) covering the whole length of the cortex (strip from the upper edge of the marginal zone to the corpus callosum) were defined using the maximum intensity Z-projection of the acquired confocal images. These cortical strips were then divided into 10 identical bins using a macro created in Image J (FIJI), and the number of cells in each bin was counted manually. The mean number of cells in each bin was calculated for each animal and expressed as a percentage of the total number of cells *per* strip unless otherwise stated. In P1 samples, since the region between the MZ and the CP (corresponding to bins 2 to 4) at this particular stage was too densely populated to be counted, only bin 1 and bins 5 to 10 were counted and represented as absolute number of cells/bin. For the BrdU counts, images were acquired, processed and quantified as described above. The width of the strips was fixed at 70 µm and the height was variable depending on the thickness of the cortex. At P1, the mean thickness *per* strip was 528 ± 63.96 µm for controls and 547.5 ± 33.53 µm for Reelin deficient mice (Unpaired t-test, t=0.4727, df=5, P=0.6564). At P30, the mean height *per* strip was 1108 ± 84.23 µm for controls and 1206 ± 116.3 µm for Reelin deficient mice (Unpaired t-test, t=1.409, df=7, P=0.2017). To obtain the profile plots, representative images were selected for each genotype and the Plot profile tool of Image J was used to generate them.

For the MGE experiment analysis, the number of Cux1+ cells in the first 50 µm of the cortex (measured from the outermost edge of the cortex) were counted in a single plane image in the MGE grafted region and the contralateral region of *GAD-Reelin*$^{F/F}$ mice.

For the apical processes orientation analysis, the angle of the apical processes respect to the pia was measured in at least 50 GFP+ neurons *per* animal. The data collected was then used to calculate the frequency distribution *per* angle and plotted in a graph.

To determine cell distribution in the hippocampus, the distribution of BrdU+ cells in the granule cell layer of the dentate gyrus (DG; BrdU at E15 and P10-P11) and the CA1 (BrdU at E12 and E15) was analyzed. The cell layers were subdivided into three layers (upper, middle and inner) and the number of BrdU+ cells in each position was counted. In the DG, the number of BrdU+ cells located in the Hilus was also counted.

The thickness of the layered hippocampal structures CA1 and DG was determined by measuring the average width of each structure in images acquired with a Nikon Eclipse E600 microscope. At least 3 images per animal were analyzed and 10 evenly spaced measures were taken in each structure to calculate the mean width.

Between 3 and 5 different animals per genotype and age were used for the above-mentioned quantifications, despite the observed phenotypes were confirmed in larger groups. Details of the exact number of mice used in each quantification are provided in the figure legends.

Statistical Analysis

All statistical analyses were performed using GraphPad Prism 6.0 software (GraphPad Software, Inc). Data were analyzed using either the two-tailed unpaired t-test or two-way ANOVA with multiple comparison post-hoc tests unless otherwise stated. Details of the sample size and statistical test used are given in each figure legend. Data in the graphs are presented as mean ± SEM and data in the text as mean ± SD. Quantification of immunostaining was performed blindly. Statistical significance was established at $p \leq 0.05$.

References

1. H. Taniguchi, *et al.*, A resource of Cre driver lines for genetic targeting of GABAergic neurons in cerebral cortex. *Neuron* **71**, 995–1013 (2011).

2. L. Pujadas, *et al.*, Reelin regulates postnatal neurogenesis and enhances spine hypertrophy and long-term potentiation. *J. Neurosci.* **30**, 4636–4649 (2010).

3. A. Cárdenas, *et al.*, Evolution of Cortical Neurogenesis in Amniotes Controlled by Robo Signaling Levels. *Cell* **174**, 590-606.e21 (2018).

4. M. Martinez-Losa, *et al.*, Nav1.1-Overexpressing Interneuron Transplants Restore Brain Rhythms and Cognition in a Mouse Model of Alzheimer's Disease. *Neuron* **98**, 75-89.e5 (2018).

5. A. K. Hadjantonakis, M. Gertsenstein, M. Ikawa, M. Okabe, A. Nagy, Generating green fluorescent mice by germline transmission of green fluorescent ES cells. *Mech. Dev.* **76**, 79–90 (1998).

6. I. Zipancic, M. E. Calcagnotto, M. Piquer-Gil, L. E. Mello, M. Alvarez-Dolado, Transplant of GABAergic precursors restores hippocampal inhibitory function in a mouse model of seizure susceptibility. *Cell Transplant.* **19**, 549–564 (2010).

7. M. Alvarez-Dolado, *et al.*, Cortical inhibition modified by embryonic neural precursors grafted into the postnatal brain. *J. Neurosci. Off. J. Soc. Neurosci.* **26**, 7380–7389 (2006).

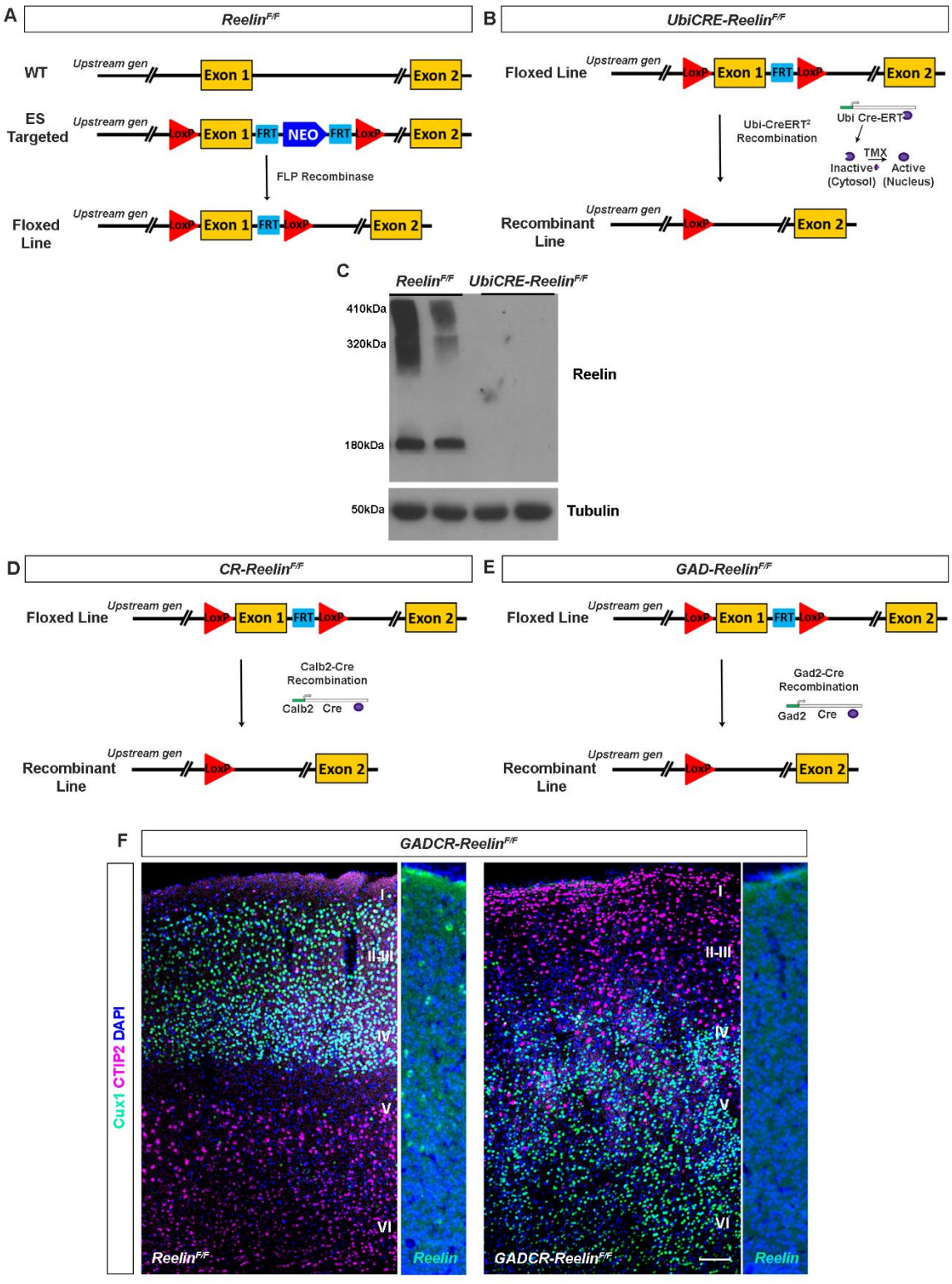

Fig. S1. *Reelin*$^{F/F}$ transgenic line generation and validation.

A, To obtain the Floxed Reelin line (*Reelin*$^{F/F}$), LoxP sites were introduced at either side of the Exon 1 of the *Reln* gene. **B**, The line was bred to homozygosity and then, to validate the model, it was crossed with *the* Ubi-Cre^{ERT2} line (*UbiCre-Reelin*$^{F/F}$), which expresses a tamoxifen-inducible

Cre recombinase under the control of the Ubiquitin promoter. P30 *UbiCre-Reelin*$^{F/F}$ mice were injected with tamoxifen intraperitoneally (180 mg/Kg) for 3 consecutive days and sacrificed 2 weeks later. **C**, Western Blot of total brain homogenates (excluding cerebellum) against Reelin protein evidence a clear reduction of Reelin protein levels in our model. **D-E**, Crossing strategy of the Reelin$^{F/F}$ line with the *Calb2*$^{tm1(cre)Zjh}$/J (**D**) and the *Gad2*$^{tm2(cre)Zjh}$/J (**E**) Cre lines to obtain cell-specific Reelin-deficient models in CR cells (*CR-Reelin*$^{F/F}$) and GABAergic interneurons (*GAD-Reelin*$^{F/F}$), respectively. **F**, To further validate our model we generated a double knockout by combining the deletion of Reelin from both CR cells and GABAergic interneurons (*GADCR-Reelin*$^{F/F}$). Analysis of the cortical lamination in this model at P30 evidenced an inverted laminar organization in the neocortex of the *GADCR-Reelin*$^{F/F}$ strongly resembling the *reeler* phenotype. Reelin IHC confirmed the complete absence of this protein in the cortex of the *GADCR-Reelin*$^{F/F}$mice (P15). Scale bar = 100µm.

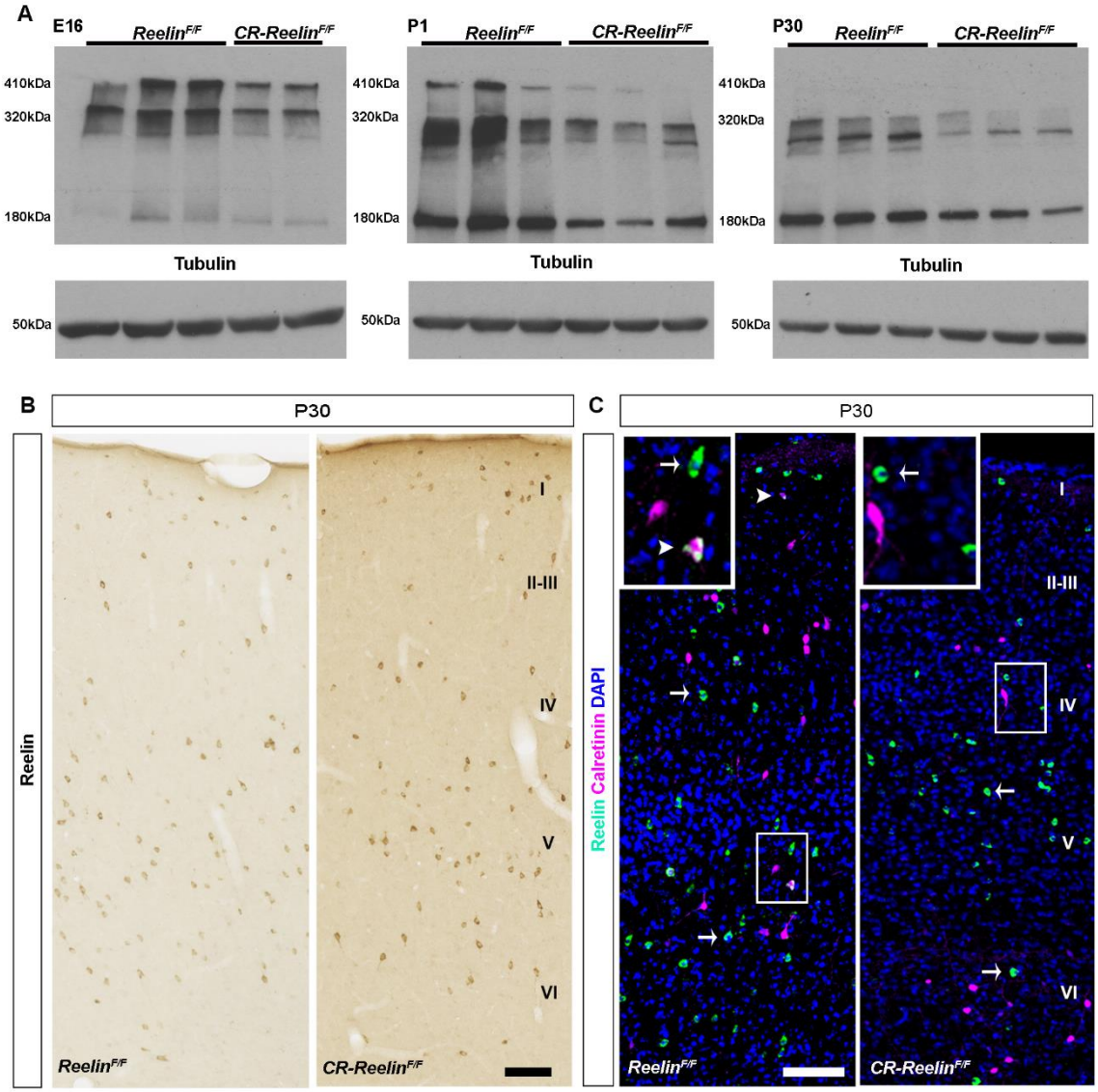

Fig. S2. Reelin expression in the cortex of the *CR-Reelin$^{F/F}$* model

A, Cortex and hippocampus brain homogenate western blot against Reelin protein at E16, P1 and P30 evidencing a decrease in Reelin levels in *CR-Reelin$^{F/F}$* brains specially at early stages. **B**, Representative photomicrograph showing the cortical distribution of Reelin at P30 in *Reelin$^{F/F}$* (left) and *CR-Reelin$^{F/F}$* mice (right). **C**, Double IHC of Reelin+ (green) and Calretinin+ cells (magenta) at P30 in the presence (*Reelin$^{F/F}$*, left) and absence (*CR-Reelin$^{F/F}$*, right) of Reelin from CR cells (arrowheads indicate double-labeled cells and arrows indicate single-labeled Reelin+ cells). Note the co-localization of Reelin and Calretinin staining in the *Reelin$^{F/F}$* but not in the *CR-Reelin$^{F/F}$* brain. Scale bar, **B-C**, 100 µm. Cortical Layer I (I), Layers II-III (II-III), Layer IV (IV), Layer V (V) and Layer VI (VI).

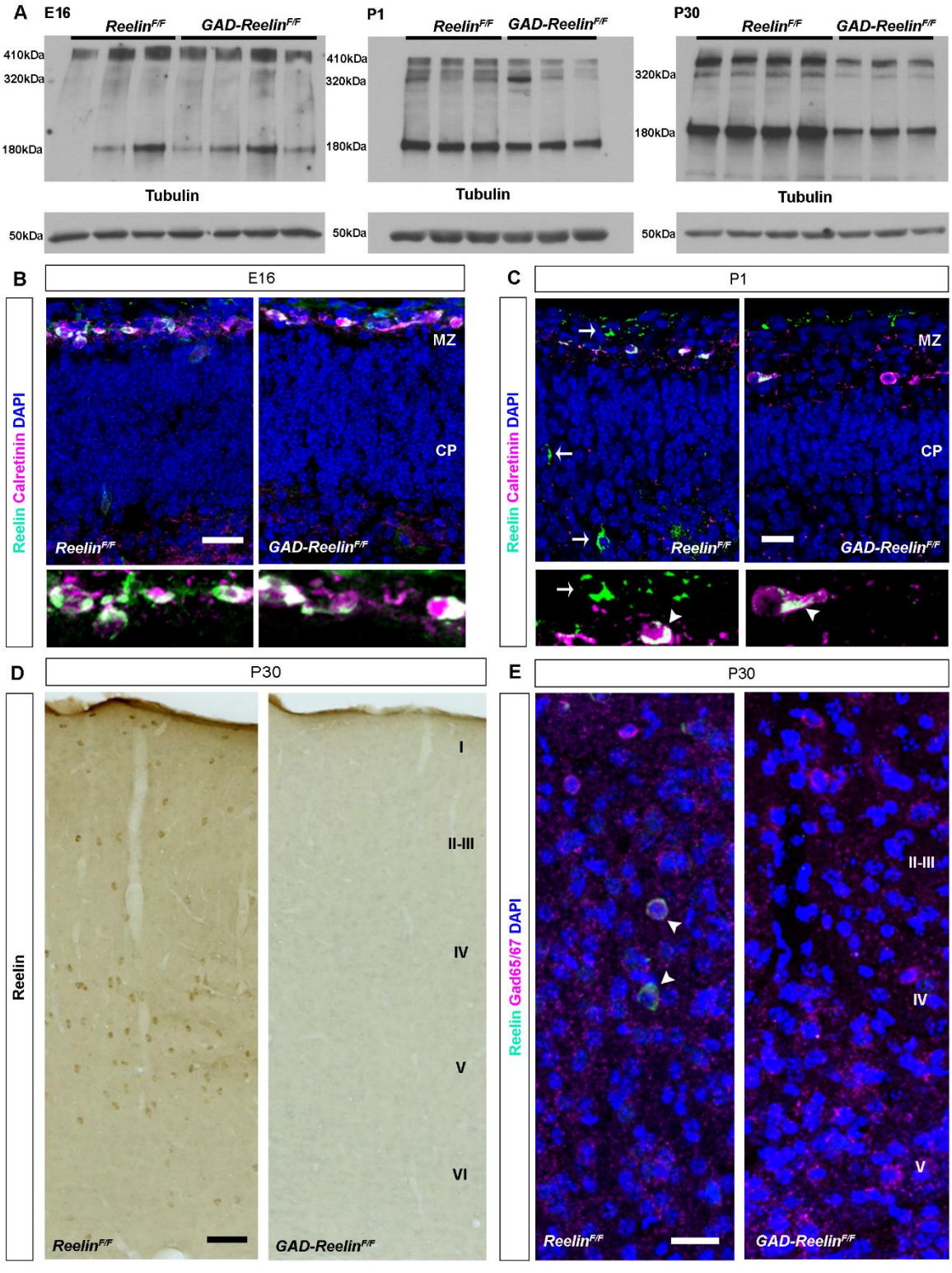
A
E16
Reelin F/F
GAD-Reelin F/F
410kDa
320kDa
180kDa
Tubulin
50kDa
P1
Reelin F/F
GAD-Reelin F/F
410kDa
320kDa
180kDa
Tubulin
50kDa
P30
Reelin F/F
GAD-Reelin F/F
320kDa
180kDa
Tubulin
50kDa
B
E16
Reelin Calretinin DAPI
MZ
CP
Reelin F/F
GAD-Reelin F/F
C
P1
Reelin Calretinin DAPI
MZ
CP
Reelin F/F
GAD-Reelin F/F
D
P30
Reelin
I
II-III
IV
V
VI
Reelin F/F
GAD-Reelin F/F
E
P30
Reelin Gad65/67 DAPI
II-III
IV
V
Reelin F/F
GAD-Reelin F/F

Fig. S3. Reelin expression in the cortex of the *GAD-Reelin$^{F/F}$* model

A, Cortex and hippocampus brain homogenate western blot against Reelin protein at E16, P1 and P30 showing a progressive decrease in Reelin levels in *GAD-Reelin$^{F/F}$* brains. **B-C**, Double IHC of Reelin+ (green) and Calretinin+ cells (magenta) at E16 (**B**) and P1 (**C**) evidencing the presence of double labeled cells corresponding to CR cells at the MZ in both *Reelin$^{F/F}$* and *GAD-Reelin$^{F/F}$* mice. Note that at P1 (**C**) Calretinin- Reelin+ cells (presumably GABAergic interneurons) start to be present in the MZ of *Reelin$^{F/F}$* but not in *GAD-Reelin$^{F/F}$* mice (arrows). Magnification of Marginal Zone cells (**B-C**, bottom). **D**, Representative photomicrograph showing cortical distribution of Reelin at P30 in *Reelin$^{F/F}$* (left) and *GAD-Reelin$^{F/F}$* (right) mice. Note the complete absence of Reelin in the cortex at this stage in *GAD-Reelin$^{F/F}$* mice. **E**, Double IHC of Reelin+ (green) and Gad65/67+ cells (magenta) at P30 further evidencing the specific depletion of Reelin from GABAergic interneurons in the *GAD-Reelin$^{F/F}$* model. Arrowheads indicate double-labeled cells. Scale bar, **B, D** 25 µm, **C,** 20 µm. Marginal Zone (MZ), Cortical Plate (CP), Cortical Layer I (I), Layers II-III (II-III), Layer IV (IV), Layer V (V) and Layer VI (VI).

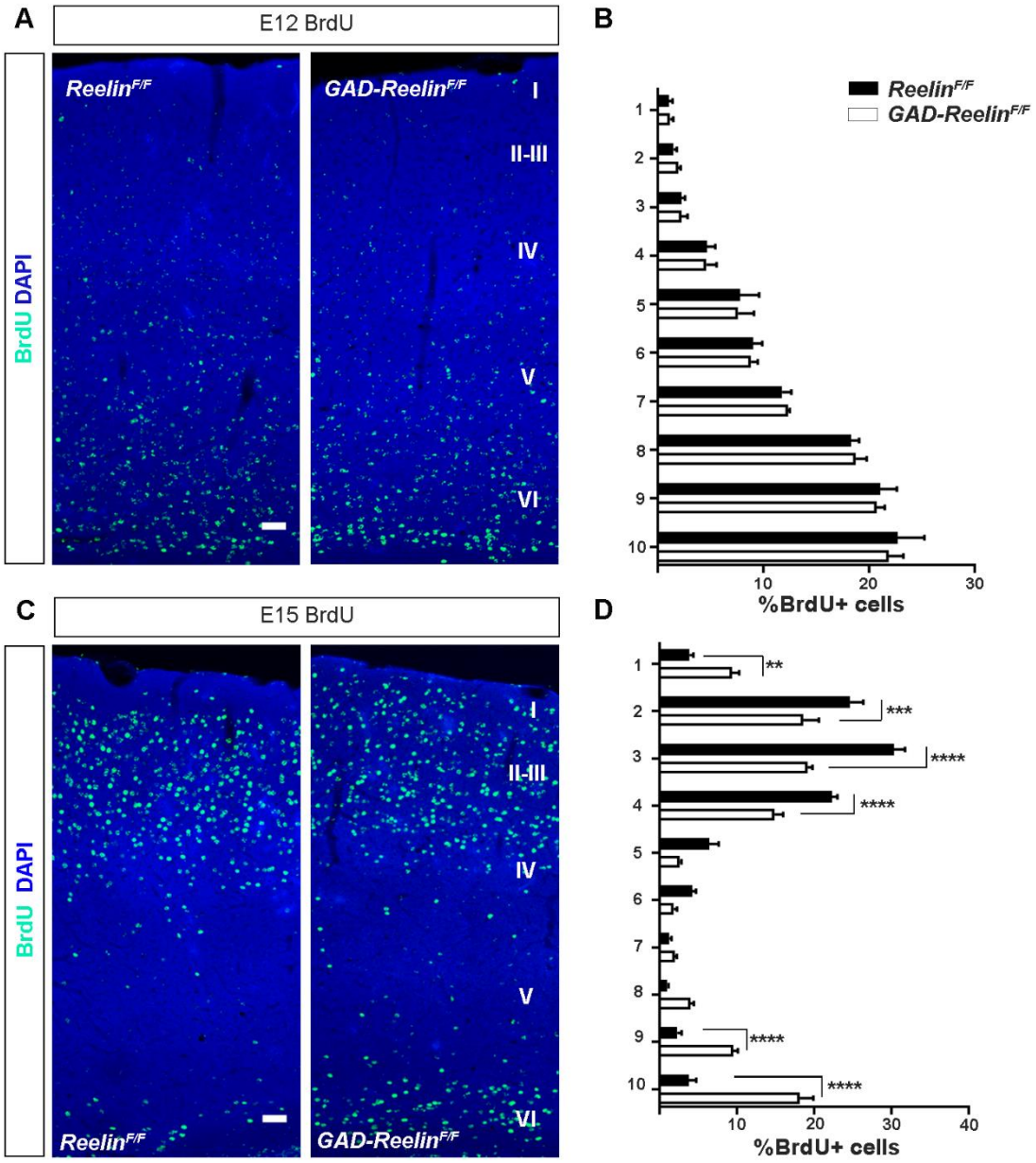

Fig. S4. Positioning of cortical cells in the absence of Reelin from GABAergic interneurons.

A, C, BrdU immunohistochemistry of P30 mice injected with BrdU at E12 (**A**) and E15 (**C**) in *Reelin*$^{F/F}$ (left) and *GAD-Reelin*$^{F/F}$ (right) mice. **B, D**, Quantification of the percentage of BrdU+ cells *per* bin in mice injected at E12 (**B**) or E15 (**D**). The results further confirm the presence of late-born neurons (E15) both in the marginal zone and in deep cortical layers in the *GAD-Reelin*$^{F/F}$ model. Data represents mean ± s.e.m. Statistical analysis **B,** Bin F (9, 60)= 114.7 p<0.0001; Two-way ANOVA with Bonferroni post hoc test; n.s., n= 4 mice per genotype; **D,** Bin x Genotype Interaction F(9, 60)= 31 p<0.0001; Two-way ANOVA with Bonferroni post hoc test; $^{**}P < 0.01$, $^{***}P < 0.001$, $^{****}P < 0.0001$, n= 4 mice per genotype. Scale bar **A**, **C**, 50 µm. Cortical Layer I (I), Layers II-III (II-III), Layer IV (IV), Layer V (V) and Layer VI (VI).

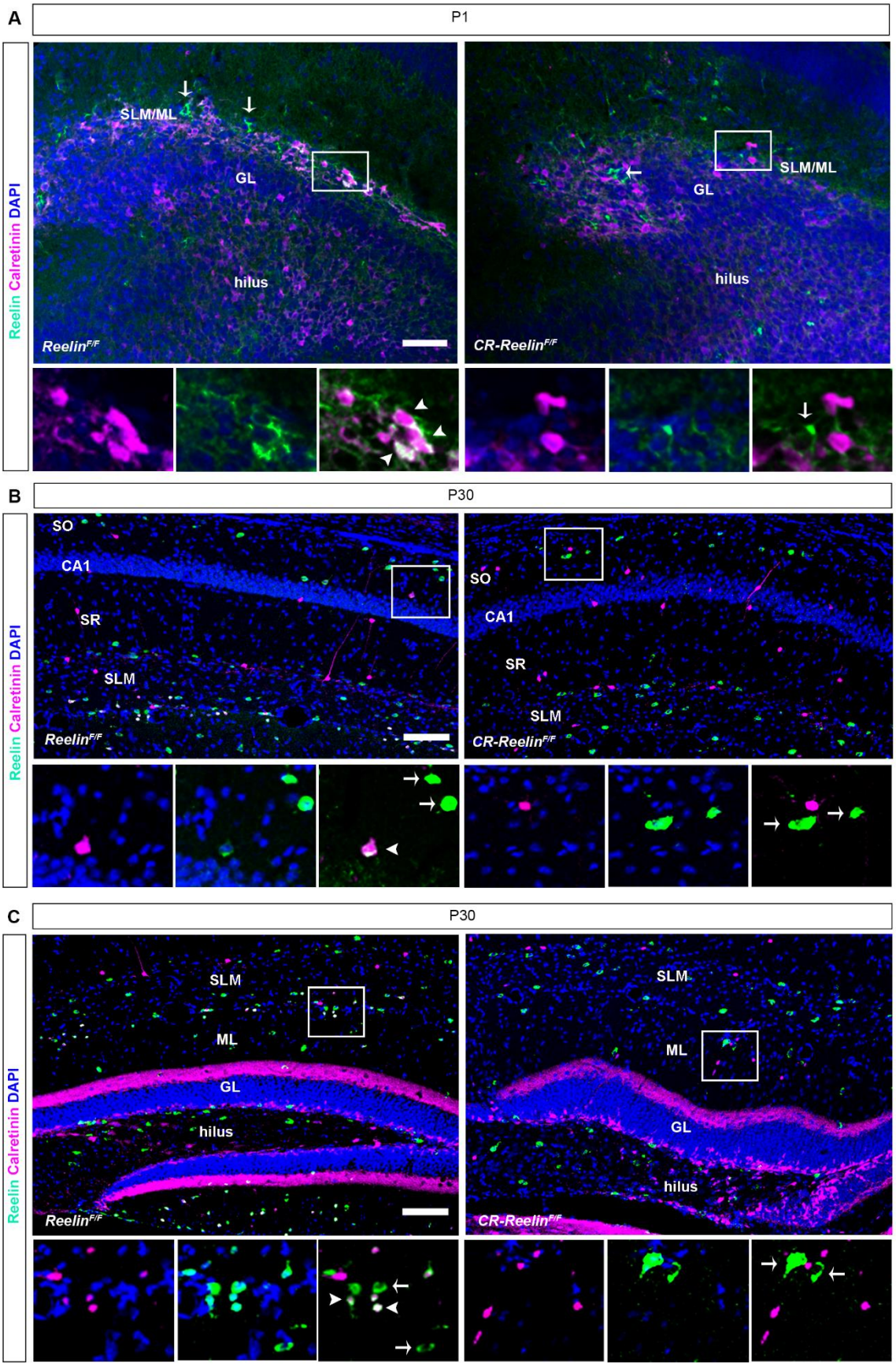
A
P1
Reelin Calretinin DAPI
SLM/ML
GL
hilus
Reelin^F/F
CR-Reelin^F/F
B
P30
SO
CA1
SR
SLM
C
ML
hilus

Fig. S5. Reelin expression in the hippocampus of the *CR-Reelin$^{F/F}$* model.

A-C, Double IHC of Reelin+ (green) and Calretinin+ hippocampal cells (magenta) at P1 (**A**) and P30 (**B-C**) in *Reelin$^{F/F}$* (left) and *CR-Reelin$^{F/F}$* (right) mice. Arrowheads indicate double-labeled cells. Images evidence the absence of double-labeled cells in the *CR-Reelin$^{F/F}$* brain at all the stages studied confirming that Reelin expression is depleted specifically in CR cells in this model. Note the presence of Calretinin-/Reelin+ cells, presumably corresponding to GABAergic interneurons, in both *Reelin$^{F/F}$* and *CR-Reelin$^{F/F}$* mice (arrows). Scale bar, **A,** 50 µm, **B-C,** 100 µm. Stratum Lacunosum Moleculare/Molecular Layer (SLM/ML), Granule Layer (GL), Cornus Ammonis (CA), Stratum Oriens (SO) and Stratum Radiatum (SR).

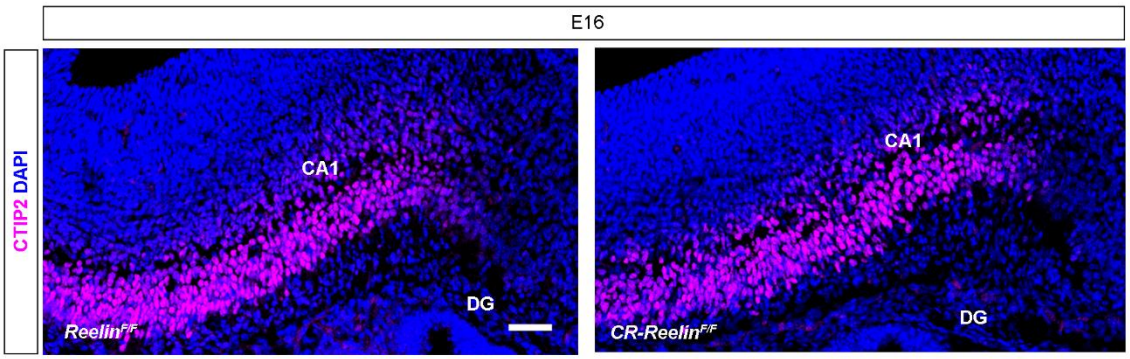

Fig. S6. Hippocampal cytoarchitecture at E16 in the absence of Reelin from CR cells.

Confocal images of the hippocampus at E16 stained with CTIP2 in *Reelin*$^{F/F}$ (left) and *CR-Reelin*$^{F/F}$ mice (right) showing a similar hippocampal organization in both genotypes. Scale bar=100 µm. Dentate Gyrus (DG) and Cornus Ammonis (CA).

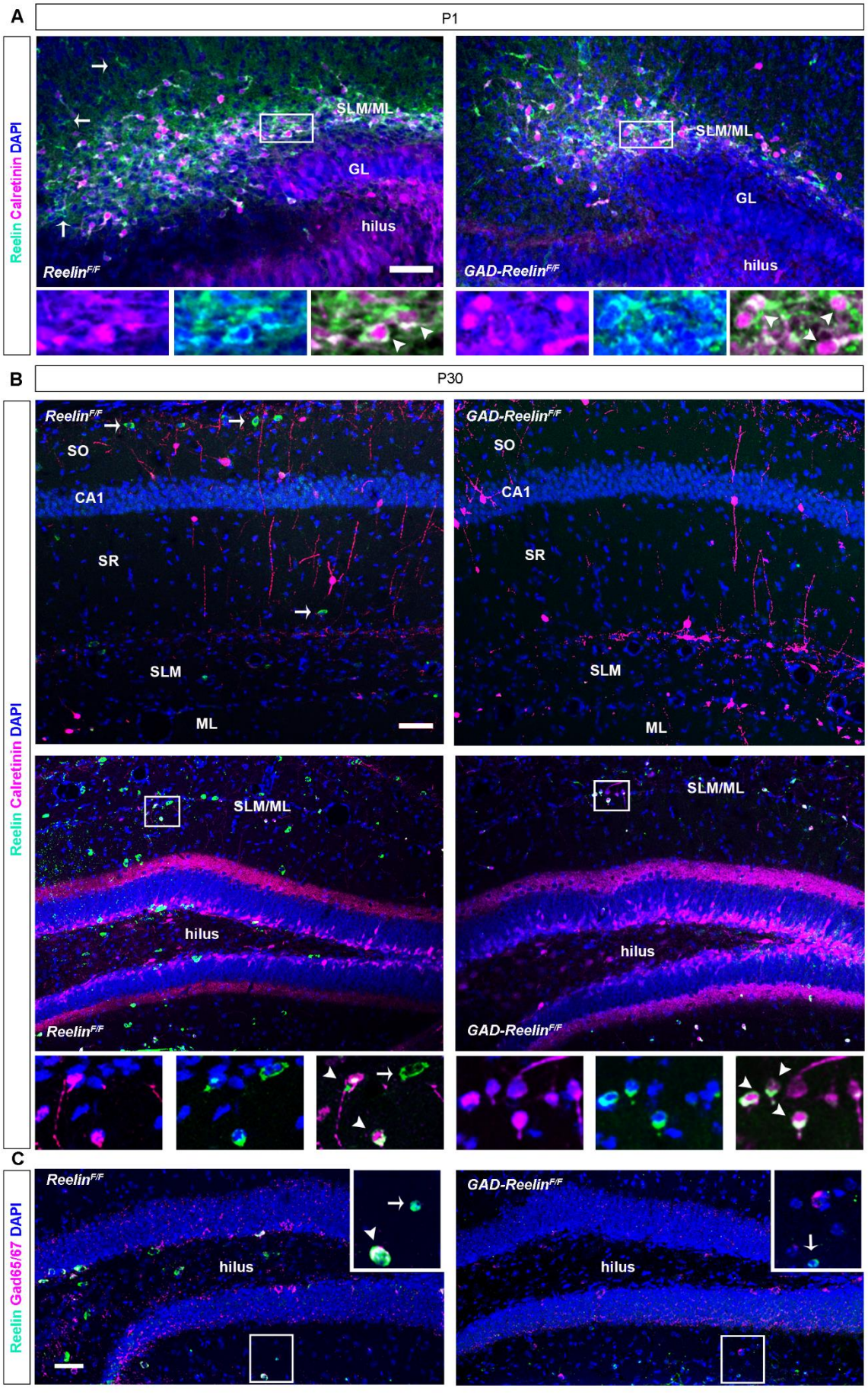
A
P1
Reelin Calretinin DAPI
SLM/ML
GL
hilus
ReelinF/F
GAD-ReelinF/F
B
P30
SO
CA1
SR
SLM
ML
C
Reelin Gad65/67 DAPI

Fig. S7. Reelin expression in the hippocampus of the *GAD-Reelin$^{F/F}$* model.

A-B, Double IHC of Reelin+ (green) and Calretinin+ cells (magenta) at P1 (**A**) and P30 (**B**) in *Reelin$^{F/F}$* (left) and *GAD-Reelin$^{F/F}$* (right) mice. Images evidence the presence of double-labeled (CR) cells in both genotypes at all the studied stages (arrowheads) and the absence of single-labeled Reelin+ cells (arrows) specifically in the *GAD-Reelin$^{F/F}$* model. **C**, Double IHC of Reelin+ (green) and Gad65/67+ cells (magenta) at P30 in *Reelin$^{F/F}$* (right) and *GAD-Reelin$^{F/F}$* (left) mice. Note the absence of double -labeled GAD65/67+ Reelin+ cells, corresponding to GABAergic interneurons, specifically in the *GAD-Reelin$^{F/F}$* model. Scale bar, **A-B** 50 µm, **C,** 100 µm. Stratum Lacunosum Moleculare/Molecular Layer (SLM/ML), Granule Layer (GL), Cornus Ammonis (CA), Stratum Oriens (SO), Stratum Radiatum (SR) and Molecular Layer (ML).

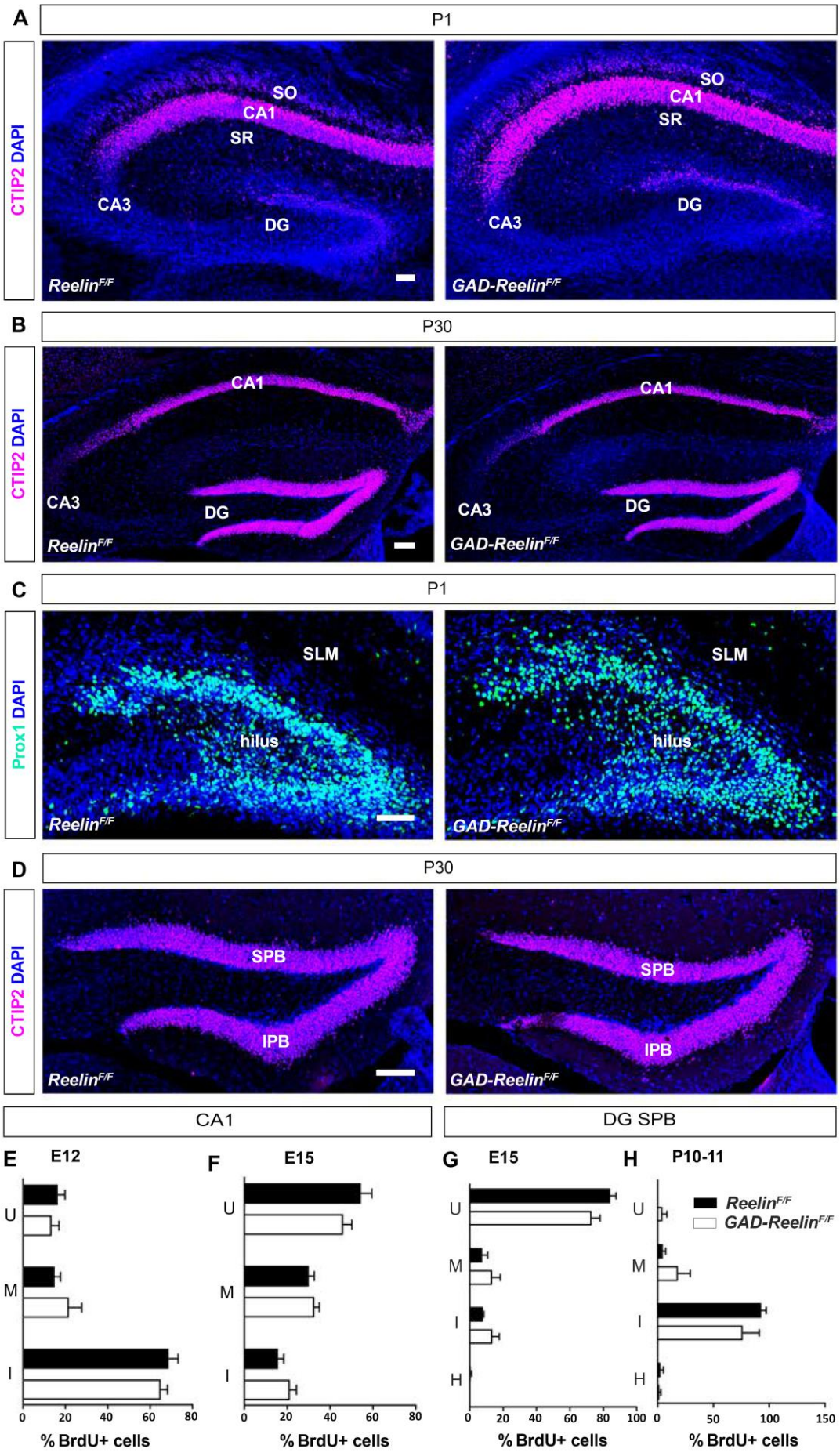
A
P1
CTIP2 DAPI
SO
CA1
SR
CA3
DG
Reelin F/F
GAD-Reelin F/F
B
P30
C
Prox1 DAPI
SLM
hilus
D
SPB
IPB
CA1
DG SPB
E
E12
F
E15
G
E15
H
P10-11
U
M
I
H
0
20
40
60
80
100
150
% BrdU+ cells

Fig. S8. Hippocampal cytoarchitecture in the absence of Reelin from GABAergic interneurons.

A-D, Representative confocal images of the hippocampus at P1 (**A**, CTIP2**; C**, Prox1) and P30 (**B,D**, CTIP2) in *Reelin*$^{F/F}$ (left) and *GAD-Reelin*$^{F/F}$ (right) mice showing no differences in the laminar organization of the CA1 and the DG. **E-F**, Analysis of BrdU+ cells distribution in the CA1 of mice injected with BrdU at E12 (**E**) or E15 (**F**). **G-H**, Analysis of BrdU+ cells distribution in the suprapyramidal blade of the DG of mice injected with BrdU at E15 (**G**) or P10-11 (**H**). Birth-dating studies further confirm the absence of significant alterations in the inside-out migration pattern of the *GAD-Reelin*$^{F/F}$ model. Data represents mean ± s.e.m. Statistical analysis **E,** Layer x Genotype Interaction $F(2, 21)= 1.051$ $p=0.3674$; Two-way ANOVA with Bonferroni post hoc test n.s.; *Reelin*$^{F/F}$ n= 5 and *GAD-Reelin*$^{F/F}$ n=4; **F**, Layer x Genotype Interaction $F(2, 18)= 2.249$ $p=0.1343$; Two-way ANOVA with Bonferroni post hoc test; n.s. n= 4 mice per genotype; **G**, Layer x Genotype Interaction $F(3, 24)= 2.887$ $p=0.0564$; Two-way ANOVA with Bonferroni post hoc test; n.s. n= 4 mice per genotype; **H**, Layer x Genotype Interaction $F(3, 20)= 1.213$ $p=0.3307$; Two-way ANOVA with Bonferroni post hoc test; n.s. *Reelin*$^{F/F}$ n= 3 and *GAD-Reelin*$^{F/F}$ n=4. Scale bar=50 µm. Cornus Ammonis (CA), Stratum Oriens (SO), Stratum Radiatum (SR), Dentate Gyrus (DG), Suprapyramidal Blade (SPB), Infrapyramidal Blade (IPB), Upper layer (U), Middle layer (M) and Inner layer (I).

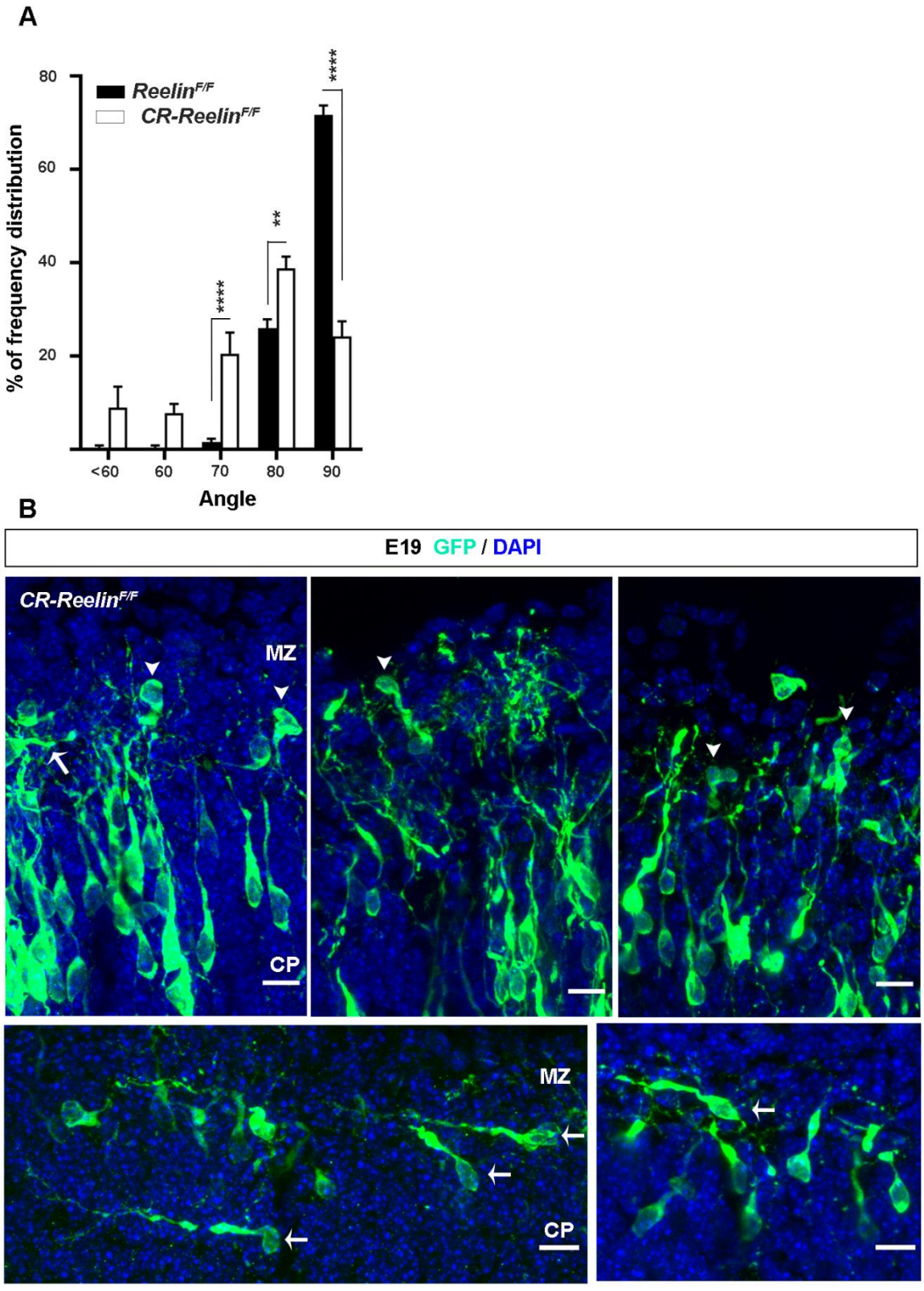

Fig. S9. Aberrant orientation of leading-like processes in E14.5-born neurons in *CR-Reelin*$^{F/F}$ mice and embryos.

A, Distribution (%) of the GFP+ apical processes orientation from embryos electroporated at E14.5 and sacrificed at P1 (A). Note that whilst most of the apical processes in *Reelin*$^{F/F}$ mice are

perpendicular to the MZ , in CR-*Reelin*$^{F/F}$ mice almost 80% of the apical processes present an oblique or even parallel orientation to the MZ. **B**, Representative confocal images of E19 GFP+ neurons evidencing the presence of basally (white arrowhead) and horizontally (white arrow) oriented leading-like processes in CR-*Reelin*$^{F/F}$ mice, suggesting that at least some ectopic neurons in the MZ might undergo inward migration at perinatal stages. Data represents mean ± s.e.m. Statistical analysis **A,** Angle x Genotype Interaction $F(4, 25)= 66.04$ $p<0.0001$; Two-way ANOVA with Bonferroni post hoc test $^{**}P < 0.01$, $^{****}P < 0.0001$; *Reelin*$^{F/F}$ n= 4 and *CR-Reelin*$^{F/F}$ n=3; Scale bar=10 µm.

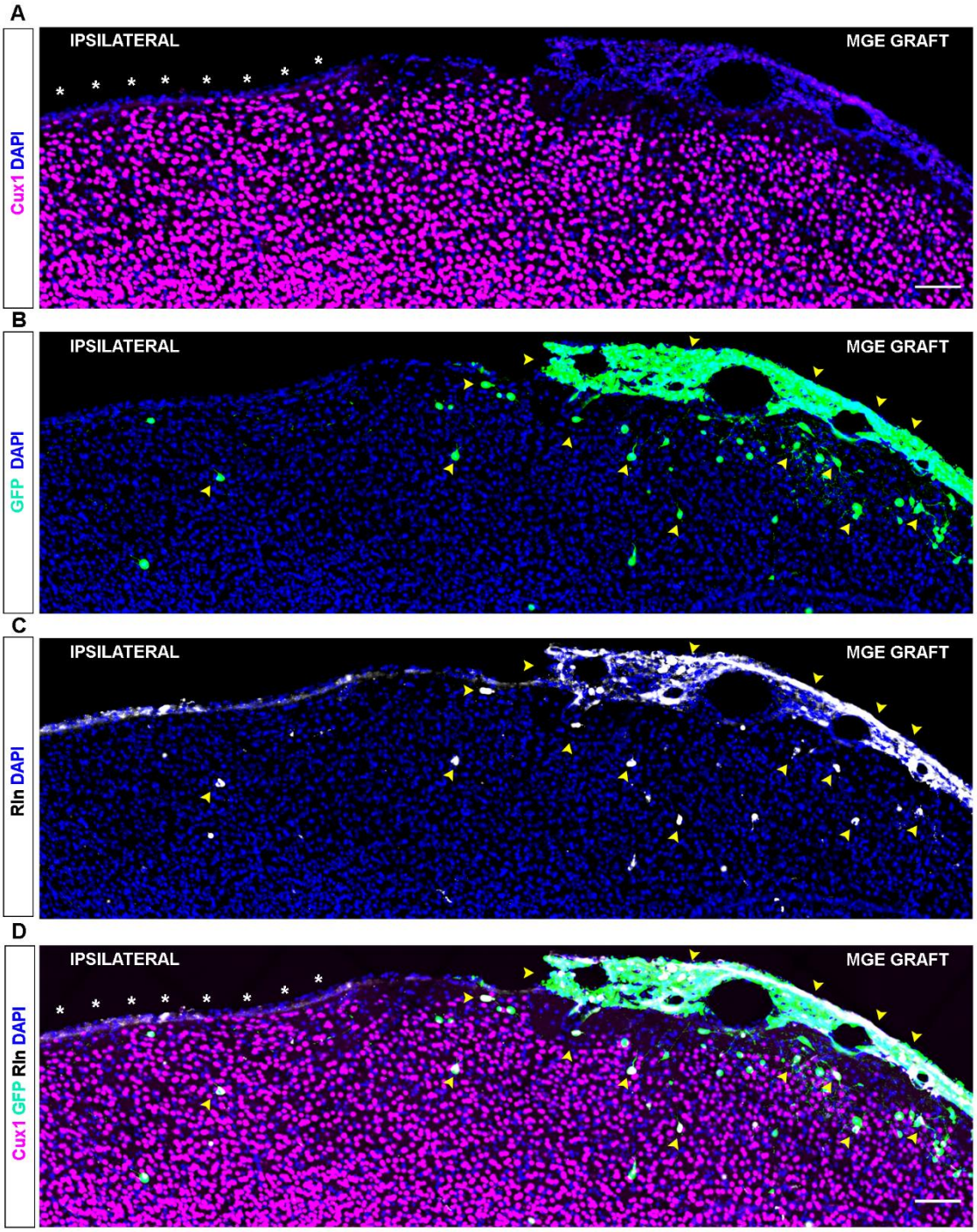

Fig. S10. Postnatal expression of Reelin in *GAD-Reelin*$^{F/F}$ mice reduces Layer I invasion.

A-D, Representative images of the ipsilateral hemisphere of a *GAD-Reelin*$^{F/F}$ mouse grafted with GFP+ MGE cells at P3 and sacrificed at P18 showing Cux1 (A), GFP (B) Reelin (C) and merged (D) immunostaining. Images evidence a decrease in the number of Cux1+ cells ectopically located in the layer I of the MGE grafted area compared to the adjacent ipsilateral hemisphere, where Cux1+ cells clearly invade layer I (asterisks). The reduction in the number of ectopic Cux1 cells is concomitant to the presence of superficial clusters of GFP+ cells that express Reelin (B-C, yellow arrowheads). Scale bar=100 µm.

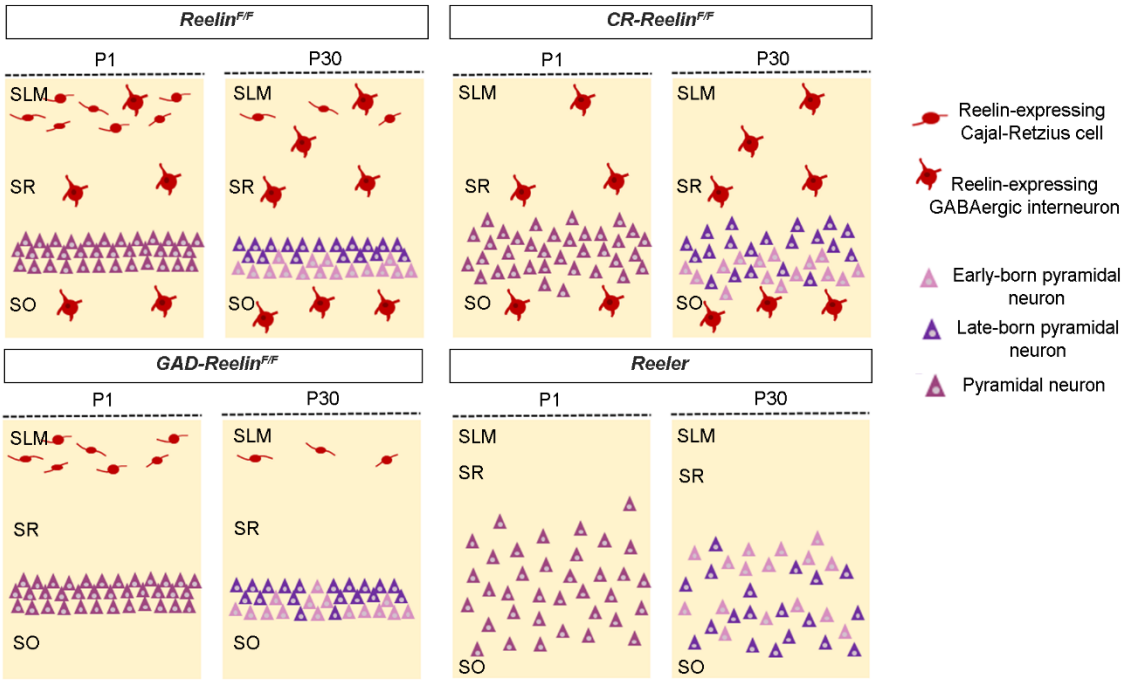

Fig. S11. Model of hippocampal CA1 lamination.

Proposed model of Reelin functions in hippocampal lamination based on the data obtained from the cell-specific Reelin-deficient models. Note that Reelin deficiency from CR cells leads to mild migratory abnormalities in the CA1 whereas Reelin deficiency from GABAergic interneurons results in a nearly normal migration and lamination. These results suggest that in the hippocampus proper, Reelin from either CR cells or GABAergic interneurons is sufficient to give rise to a nearly normal hippocampal cytoarchitecture, far different from that found in *Reeler* mice, indicating a compensation/cooperation between these two sources of Reelin in the hippocampus proper. These effects are in sharp contrast to those observed in the DG, where GABAergic interneuron-derived Reelin is able to compensate some, but not all, the migratory defects caused by the lack of Reelin from CR cells, indicating in this case a cell-specific effect of Reelin in the morphogenesis of the DG. Stratum Lacunosum Moleculare (SLM), Stratum Oriens (SO) and Stratum Radiatum (SR).